12-1-2021

SEARCH FOR LOW MASS DARK MATTER USING LEPTOPHILIC GAUGE BOSON MODEL IN NEUTRINO EXPERIMENTS: MINIBOONE AND DUNE

Gajendra Gurung

SEARCH FOR LOW MASS DARK MATTER USING LEPTOPHILIC GAUGE BOSON MODEL IN NEUTRINO EXPERIMENTS: MINIBOONE AND DUNE

by

GAJENDRA GURUNG

Presented to the Faculty of the Honors College of

The University of Texas at Arlington in Partial Fulfillment

of the Requirements for the Degree of

HONORS BACHELOR OF SCIENCE IN PHYSICS

UNIVERSITY OF TEXAS AT ARLINGTON

December 2021

DEDICATION

To my Parents, Bijay Gurung and Bal Maya Gurung, who never had any formal education but made sure to do everything so that I could go to school.

To Sanjay Shah, my secondary school mathematics teacher, who believed in me and gifted me with books so that I never stopped learning.

ACKNOWLEDGMENTS

This thesis would never have existed if it were not for the support of countless people in my life.

Principally, I would like to thank my faculty advisor, Dr. Jaehoon Yu, and postdoctoral researcher, Dr. Wooyoung Jang for their guidance and support throughout this research.

I would like to thank Dr. Francesco Capozzi[1], Dr. Ian Shoemaker[2], Adrian Thompson[3]and Dr. Bhaskhar Dutta[3] for their patience and support by letting me join their research collaboration.

I would like to acknowledge the support and discussions with Dr. Andrew Brandt, Aayush Bhattarai, Ahmed Bedair, Steven Boucher, Cristobal Garces, Harshwardhan Prasa, Skyler Ryu, and Michael Solek. Thanks for being immensely supportive of my work.

Finally, I would like to thank Caitlin Zainz for her encouragement and patience.

December 23, 2021

[1]Instituto de Física Corpuscular, Valencia, Spain
[2]Virginia Polytechnic Institute and State University, Blacksburg, VA
[3]Mitchell Institute for Fundamental Physics and Astronomy, Texas A & M, College Station, TX

ABSTRACT

Search for Low Mass Dark Matter Using Leptophilic Gauge
Boson Model in Neutrino Experiments:
MiniBooNE and DUNE

Gajendra Gurung, B.S. Physics

The University of Texas at Arlington, 2021

Faculty Mentor: Jaehoon Yu

Dark Matter (DM) is a form of matter that makes about 25% of the universe as indicated by cosmological evidence, like weak gravitational lensing, cosmic microwave background, rotation of spiral galaxies, etc. Despite its abundance, DM limitedly interacts with light or normal matter, thus, it is difficult to study and detect. In search of DM, we go beyond the Standard Model (SM) of Particle Physics by introducing models with particles that only interact weakly with known SM particles. We study different models and search for signatures of such particles in the proton dump mode of neutrino experiments, such as the Mini Booster Neutrino Experiment (MiniBooNE) and the near detector of the Deep Underground Neutrino Experiment (DUNE). Neutrinos are elementary particles with spin-$\frac{1}{2}$ and a neutral charge. They come in three flavors: electron, muon, and tau neutrinos. They are elusive because they only interact via weak force and gravity. One of the promising anomaly-free models, which fits the description of low-mass DM is an extension of the Standard Model featuring a gauge boson Z'. Z''s are leptophilic bosons belonging to U(1) gauge group, which gauges the differences in the lepton number as $L_\mu - L_e$, $L_e - L_\tau$ and $L_\mu - L_\tau$. Such low-mass Z''s are also able to explain the measured value of the muon's anomalous magnetic

moment. We look at the production of Z''s through meson decay, electron bremsstrahlung, and resonant production by e^+e^-collision. In this model, we look for electron-like and photon-like signatures as Z' decays into $e^\pm$ and $\mu^\pm$. We analyze the existing proton beam dump data from MiniBooNE, and GEANT-based simulation data of DUNE near detector to achieve competitive constraints on the gauge coupling parameter $g_{Z'}$ of Z'. This enables us to forward the understanding of DM. In our work, we found a considerable increase in the expected number of Z' passing through the MiniBooNE and DUNE detectors. The larger Z' production is enough to suggest that DUNE could potentially probe new areas of parameter space, which is a qualitative improvement from previously published works.

TABLE OF CONTENTS

LISTS OF ILLUSTRATIONS

NOMENCLATURE

SM	Standard Model
DM	Dark Matter
MiniBooNE	Mini Booster Neutrino Experiment
DUNE	Deep Underground Neutrino Experiment
FNAL	Fermi National Accelerator Laboratory
BSM	Beyond the Standard Model
POT	Protons on Target
PMT	Photo Multiplier Tubes
LBNE	Long Baseline Neutrino Experiment
SBNE	Short Baseline Neutrino Experiment
L_α	Lepton number, $\alpha = e, \mu, \tau$
MC	Monte Carlo

CHAPTER 1

INTRODUCTION

1.1 Background and Motivation

Elementary particle physics is a branch of physics that deals with the fundamental constituents of matter (or energy). Particle physics studies the fundamental building blocks of matter and how they interact. For example, the electrons cannot be further broken down into other particles. To study and produce these fundamental particles we need particle accelerators at very high energy (ranging from GeV to TeV) to collide particles. Only then can heavier fundamental particles be produced and detected. Thus, particle physics is also known as high-energy physics.

All the known elementary particles, including the force carriers that mediated three out the four forces (strong, weak, and electromagnetic force), can be classified and listed into a concise table called the Standard Model (SM). The Standard Model thus could be considered the periodic table for the elementary particles. The SM is currently the up-to-date theory that tends to describe the nature of the matter in the universe and can be tested in a laboratory.

On one hand, Einstein's General Theory of Relativity has stood the test of time and has been experimentally verified by observations of Cosmic Microwave Background (CMB) and Weak Gravitational Lensing; however, it does not intertwine our current understanding of the nature of particles from the SM of Particle Physics. Cosmological and astrophysical observations of the rotational speed of spiral galaxies hint towards the existence of unknown matter in the universe, which we have now denoted with the label of "Dark Matter". DM comprises about 25% of the universe, but since it does not interact copiously with normal matter or light, they are very difficult to detect and study. From the SM point of view, currently, there are anomalies related to the magnetic moment of muons [1] and charge-parity violation problems [2], low energy excess in

short baseline neutrino experiments like MiniBooNE [3], etc. These suggest that there are particles that are not described by the SM, which could be successful candidates for DM. Therefore, we must look for new frontiers of Physics and go beyond the SM.

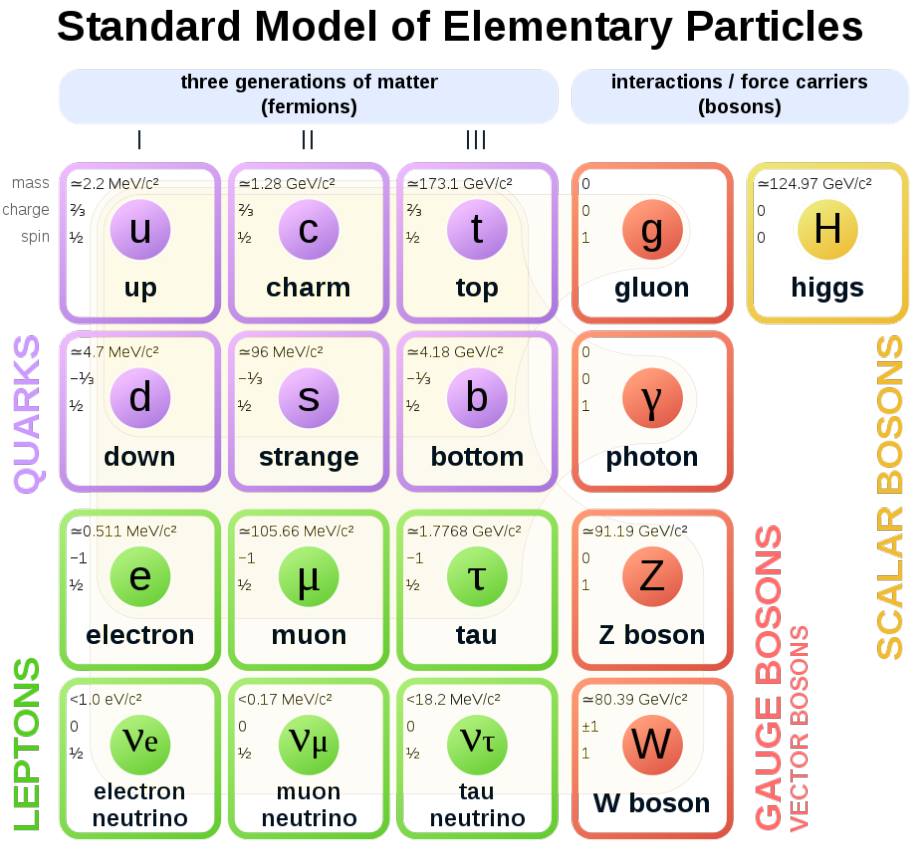

Figure 1.1: The elementary particle table of the Standard Model

1.1.1 Dark Sector and Z'

Particles in the SM are shown in Figure 1.1. The simplest of all SM model extensions is the addition of Z' gauge boson to the list of elementary particles. One of the key theoretical motivations of Z' is the possible explanation of the long-standing muon $(g-2)$ anomaly [4, 5]. Furthermore, Z''s are also well-motivated because it helps to explain the $\sim 3\sigma$ tension between the measured values of the Hubble Constant, H_0. The value of Hubble Constant, H_0, as determined from local measurements, varies from the value measured using the temperature anisotropies of the CBM [6]. The Z''s are a special type of Z bosons that also mediate the electro-weak interaction.

They are called gauge bosons because they are spin-1 particles like the photon, gluon, W, and Z, and their interactions are understood by the use of gauge symmetries (gauge invariances) described by Yang-Mills types of theories. Particularly, the Z' we are considering arises by gauging the difference in the family-lepton numbers as

$$L_1 = L_e - L_\mu, \quad L_2 = L_e - L_\tau, \quad \& \quad L_3 = L_\mu - L_\tau$$

L_1 , L_2, and L_3 are the global symmetry generators. The gauging of these family-lepton numbers does not need any additional fermions than the ones present in the SM; therefore, they are considered to be anomaly-free [7]. The gauging of such symmetries requires the extension of the SM Lagrangian by:

$$\mathcal{L} = \mathcal{L}_{SM} - \frac{1}{4} Z'^{\delta\eta} Z'_{\delta\eta} + \frac{m_{Z'}^2}{2} Z'_\delta Z'^\delta + Z'_\delta J^\delta_{\alpha-\beta} \tag{1.1.1}$$

where, $\alpha, \beta = e, \mu, \tau$, where $m_{Z'}$ is the mass of the new gauge boson and $J^\delta_{\alpha-\beta}$ is a current defined as

$$J^\delta_{\alpha-\beta} = g_{\alpha\beta}(\bar{l_\alpha}\gamma^\delta l_\alpha + \bar{\nu_\alpha}\gamma^\delta P_L \nu_\alpha - \bar{l_\beta}\gamma^\delta l_\beta - \bar{\nu_\beta}\gamma^\delta P_L \nu_\beta) \tag{1.1.2}$$

with $g_{\alpha\beta}$ being the coupling between Z' and both charged leptons l_α and the neutrinos ν_α. $P_L = \frac{1}{2}(1 - \gamma_5)$ is the left chirality projector. The symmetries of the model allow for kinetic mixing between the Z' and the SM gauge bosons. This corresponds to the following extra term of the Lagrangian

$$\mathcal{L}_\epsilon = -\frac{\epsilon}{2} F_{\gamma\delta} Z'^{\gamma\delta} \tag{1.1.3}$$

where $F_{\gamma\delta}$ is the field strength of the hypercharge [8].

The major phenomenological consequence of gauging $U(1)_{L_1}$ or $U(1)_{L_2}$ or $U(1)_{L_3}$ is the existence of neutral gauge bosons, which we call Z'_1, Z'_2 and Z'_3 respectively [9]. The difference between Z'_1 and Z'_2 is that the former couples to μ's and ν_μ's, while the latter couples to τ's and ν_τ's. Thus, Z'_1 boson effects would add a nonstandard contribution to $e^+e^- \to \mu^+\mu^-$ while leaving the corresponding process involving τ's in the final state to standard neutral-current effects [7]. Z' contribution to $e^+e^- \to \mu^+\mu^-, \tau^+\tau^-$ is shown in Figure 1.2.

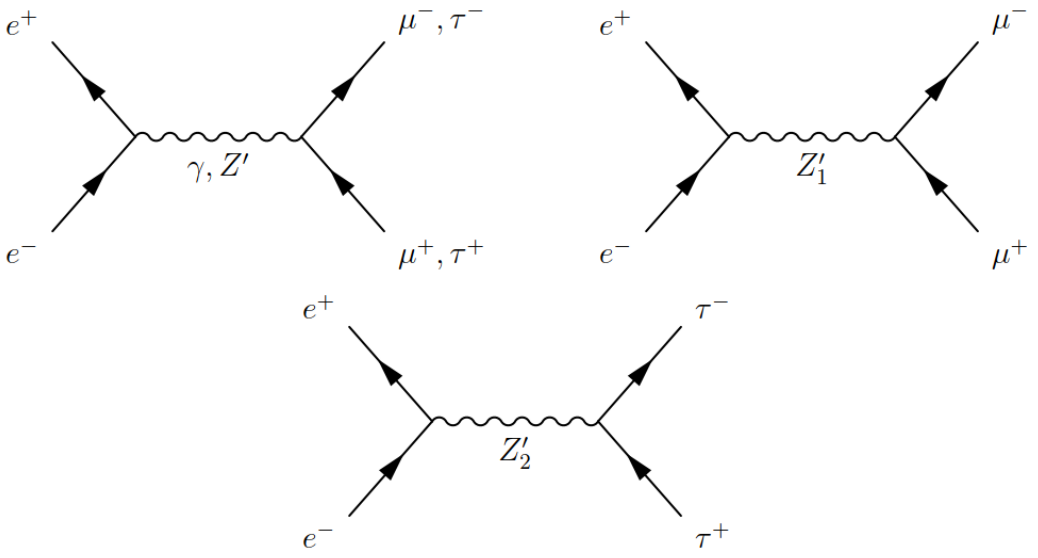

Figure 1.2: The contributions of γ, Z', & $Z'_{1,2}$ to $e^+e^- \to (i)\mu^+\mu^-, (ii)\tau^+\tau^-$

In this work, we would like to analyze the production and decay of Z', and look at the prospects of the MiniBooNE off-target mode and the DUNE near detector being able to detect such Z' bosons.

CHAPTER 2

THE SEARCH FOR Z' BOSONS IN NEUTRINO EXPERIMENTS

Neutrinos have drawn much attention in research because of their elusiveness and many unanswered questions, like what gives them masses, or are they Dirac or Majorana particles, etc. Experiments that study the properties of neutrinos are in the realm where new physics is probable. The scale of energy and size of the detector may make it possible for us to detect particles that are not described in the SM. Thus, the primary focus of this paper is the estimation of other Beyond the Standard Model (BSM) particles, like the Z' in neutrino experiments. We are focusing on two experiments, MiniBooNE and DUNE, as they are sensitive to a variety of BSM physics, including heavy neutral leptons [10–14], axion-like particles [15, 16], dark matter [12, 17–23], and millicharged particles [24]. Finally, we note that additional, complementary signatures of Z's can arise from modifications to the neutrino scattering cross-section [25, 26].

2.1 Production channels of Z'

The secondary particles we are interested in are photons and electron/positron-like signatures. In regards to the leptophilic gauge boson, each photon can be substituted by a Z' where it is kinematically allowed. In particular, we consider photons from neutral meson decays and electron bremsstrahlung. On the other hand, positrons can lead to resonant production of Z' through on-shell annihilation with electrons. The production of Z' production through Compton scattering [27] is not considered since it does not change our conclusions in the relevant region of the parameter space.

2.1.1 Neutral Meson Decay

Neutral mesons such as π^0 and η^0 created in nuclear reactions decay to a pair of SM photons where one of the photons may be replaced by the gauge boson Z'. The π^0's are boosted toward

the forward direction, the detectors located in the backward direction do not benefit from this production mechanism much, if the incoming beam is highly energetic.

The number of Z' in the ij-th bin produced by neutral meson decays can be estimated by

$$N_{Z'}^{M,ij} = N_{\gamma}^{M,ij} \frac{1}{2} \frac{\mathrm{Br}(M \to \gamma Z')}{\mathrm{Br}(M \to \gamma\gamma)}\,, \tag{2.1.1}$$

where $M = \pi^0, \eta^0$ and $Br(M \to \gamma Z')$ is the branching ratio of the neutral meson decaying into a photon and a Z', given by

$$\mathrm{Br}(M \to \gamma Z') = 2\epsilon^2(m_{Z'}^2) \left(1 - \frac{m_{Z'}^2}{m_M^2}\right)^3 \mathrm{Br}(M \to \gamma\gamma)\,, \tag{2.1.2}$$

where ϵ as

$$\epsilon(q^2) = \frac{e g_{\alpha\beta}}{2\pi^2} \int_0^1 dx\, x(1-x) \log\left(\frac{m_\alpha^2 - x(1-x)q^2}{m_\beta^2 - x(1-x)q^2}\right), \tag{2.1.3}$$

where e is the electric charge, m_α is the mass of a charged lepton and q^2 is the momentum transfer.

We take $\mathrm{Br}(\pi^0 \to \gamma\gamma) = 0.98823$ and $\mathrm{Br}(\eta^0 \to \gamma\gamma) = 0.3941$ [28]. Note that Equation 2.1.1 is only valid as a first approximation. However, the flux $N_\gamma^{M,ij}$, which we obtain from GEANT, not only includes the primary photons from meson decays, but also the secondary ones produced in the showers. Nevertheless, Equation 2.1.1 represents a more conservative estimate of the number of Z', which is not dominantly produced from meson decays.

In general, we find that the production channel from meson decays is almost negligible, but it provides a useful term of comparison with the results available in the literature.

2.1.2 Bremsstrahlung

To calculate the number of Z' in the ij-th bin produced by electron and positron bremsstrahlung, we adopt the same approach proposed in [29]

$$N_{Z'}^{\mathrm{brem},ij} = N_{\gamma}^{\mathrm{brem},ij} \left(\frac{g}{e}\right)^2 f\left(\frac{m_{Z'}}{\langle E_e \rangle}\right)\,, \tag{2.1.4}$$

where e is the electric charge, the function $f(x) = 1154\exp(-24.42x^{0.3174})$ is taken from Figure 9 in [29] and represents a phase space factor, and $\langle E_e \rangle = 1.0773E_\gamma + 13.716\,[\text{MeV}]$ is the average electron or positron energy. g is the coupling strength to electron and positrons, which depends on the model under consideration: $g = g_{\mu e}\,(g_{e\tau})$ for $L_\mu - L_e$ ($L_e - L_\tau$), $g = e\,\epsilon(m^2_{Z'})$ for $L_\mu - L_\tau$.

2.1.3 Resonant Production

A Z' can be produced on-shell through the process $e^+ + e^- \to Z'$ when $E^{\text{res}}_{e^+} = E^{\text{res}}_{Z'} = m^2_{Z'}/2m_e$. In this case, the number of Z' in the j-th angular bin is given by

$$N^{\text{res},j}_{Z'} = \frac{ZX_0}{m_p A}\sum_i \int_0^{t_{\max}} dt N^{ij}_{e^+} I(E_i, E^{\text{res}}_{e^+}, t)\sigma_{\text{res}}\,, \tag{2.1.5}$$

where A and Z are the mass and atomic number of the nuclei in the proton beam target (or beam dump), respectively, X_0 is the radiation length of the same target, m_p is the mass of the proton, $I(E_i, E_{e^+}, t)$ is the probability that a positron with initial energy E_i (the average energy of the i-th bin) has a final energy E_{e^+} after propagating t radiation lengths, and $t_{\max}$ is the maximum number of radiation lengths traveled by a positron in the target. The latter probability is taken from Ref. [30]. σ_{res} is the cross-section for resonant production and is given in [27].

$$\sigma_{\text{res}} = \frac{\pi g^2}{2m_e}\delta\left(E_{e^+} - \frac{m^2_{Z'}}{2m_e}\right)\,, \tag{2.1.6}$$

where, $g = g_{\mu e}\,(g_{e\tau})$ for $L_\mu - L_e$ ($L_e - L_\tau$), $g = e\,\epsilon(m^2_{Z'})$ for $L_\mu - L_\tau$.

For the case of DUNE, we use a single value for $t_{\max}$, regardless of the original production point of positrons in the target. This average ($t_{\max}$) is calculated as the radiation lengths of the target downstream of the 50% positron production point. The final result is $t_{\max} = 3.3$. In the case of MiniBooNE, considering that secondary particles are propagating through the relatively thick beam dump, we take $t_{\max} = 5$.

2.2 Z' decays in the detector

At tree level, Z' gauge bosons will decay to pairs of neutrinos (with their flavors corresponding to the gauged lepton number), or pairs of charged leptons $Z' \to l^+_\alpha l^-_\alpha$ and $Z' \to l^+_\beta l^-_\beta$. The number

of leptons ($l = e, \mu$) produced by $Z' \to l^+l^-$ decays in the detector is given by

$$N_l = \sum_j N_{Z'}^{\text{res},j} n_l P_{Z' \to l^+l^-}(E_{Z'}^{\text{res}}, \theta_j) + \sum_{i,j} n_l \left(N_{Z'}^{\text{brem},j} + N_{Z'}^{\pi^0,\eta^0,j} \right) P_{Z' \to l^+l^-}(E_{Z'}^{i}, \theta_j) \quad (2.2.1)$$

where $n_l = n_l(E_{Z'}, E_l^{\text{th}}, \theta_1, \theta_2)$ is the number of leptons per Z' decay with an energy E_l greater than the detection threshold E_l^{th} and going into an angle cone between θ_1 and θ_2, $E_{Z'}^{\text{res}}$ is the energy of the Z' for resonance production, $E_{Z'}^{i} = \frac{1}{2}(E_i^{\min} + E_i^{\max})$ is the center of the i-th energy bin, and $P_{Z' \to l^+l^-}$ is the probability that a Z' decays inside the detector. The latter is calculated with the Equation 2.2.2.

$$P_{Z' \to l^+l^-}(E_{Z'}, \theta) = \left(1 - e^{-\frac{L(\theta)\Gamma(Z' \to l^+l^-) m_{Z'}}{p_{Z'}}} \right) e^{-\frac{d(\theta)\,\Gamma(Z' \to l^+l^-) m_{Z'}}{p_{Z'}}} \frac{\Gamma(Z' \to l^+l^-)}{\Gamma_{\text{tot}}}, \quad (2.2.2)$$

where $L(\theta)$ is distance traveled in the detector, which depends on the Z' propagation angle θ, $d(\theta)$ is the distance traveled between the target (or beam dump) and the detector, $p_{Z'}$ is the momentum of the Z', Γ_{tot} and $\Gamma(Z' \to l^+l^-)$ are the total and partial decay widths, respectively.

In Equation 2.2.2, the sum over j is performed considering only those propagation directions of the Z' within the detector coverage, i.e. those having a propagation angle with respect to the beam $\theta_{Z'} < \theta_{\text{det}}$. Assuming the symmetry axis of a detector is aligned with the direction of the beam and that it has a width $2w$, we can estimate its angular size as $\theta_{\text{det}} \sim w/d$.

2.3 Mini Booster Neutrino Experiment (MiniBooNE)

A schematic drawing of the MiniBooNE experiment at Fermi National Accelerator Laboratory (FNAL) is shown in Figure 2.1 [31]. The Booster delivers 8 GeV kinetic energy protons that interact in a 71 cm long Beryllium target located at the upstream end of a magnetic focusing horn.

The horn pulses with a current of 174 kA and, depending on the polarity, either focuses π^+ and K^+ and defocuses π^- and K^- to form a pure neutrino beam, or focuses π^- and K^- and defocuses π^+ and K^+ to form a somewhat pure anti-neutrino beam. The produced pions and kaons decay in a 50 m long pipe, and a fraction of the neutrinos and anti-neutrinos interact in the MiniBooNE detector, which is located 541 m downstream of the Be target. A dedicated run in beam-dump

mode was carried out from November 2013 to September 2014, collecting a total of 1.86 $\times 10^{20}$ Protons on Target (POT).

The MiniBooNE detector consists of a 12.2 m diameter spherical tank filled with approximately 800 tons of mineral oil (CH_2). A schematic drawing of the MiniBooNE detector is shown in Figure 2.1. There are a total of 1280 8-inch detector phototubes covering 10% of the surface area and 240 veto phototubes. The fiducial volume has a 5 m radius and corresponds to approximately 450 tons.

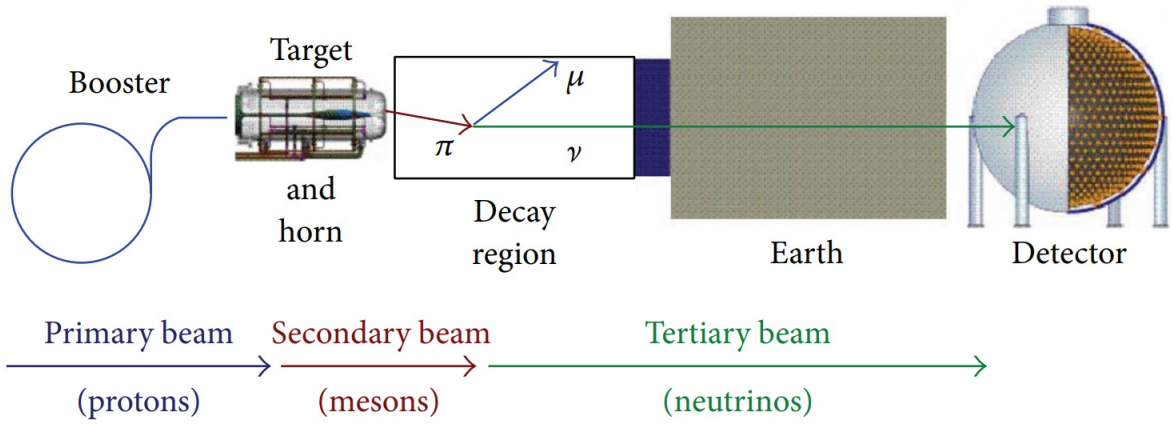

Figure 2.1: A schematic drawing of the MiniBooNE experiment. The protons beam is generated at the booster and shot into the target inside the magnetic focusing horn. The collision on the target produces mesons which decay, producing neutrinos. The neutrinos travel through dirt and are detected in the detector

2.4 Deep Underground Neutrino Experiment (DUNE)

DUNE is a long baseline neutrino experiment. The target is a 1.5 m long cylindrical graphite target 1.7 cm in diameter. The newly upgraded particle accelerator, called PIP-II, located at long baseline neutrino facility (LBNF), will produce the world's most high-intensity neutrino beamline for DUNE. The Main Injector will provide accelerated protons of about 120 GeV. The proton beam hits the graphite target. The collision with the nuclei breaks the nuclei into charged pions (π^+ and π^-) and neutrons. Then, a horn magnet is used to select the π^+'s and focuses them into a narrow beam into a decay pipe. The length from target position (MC Zero) to the end of the decay pipe is 221 m, out of which 27 m is the target chase and 194 m is the target pipe itself filled with Helium gas. Inside the 4 m inner diameter decay pipe, the π^+ spontaneously decay into μ and ν_μ.

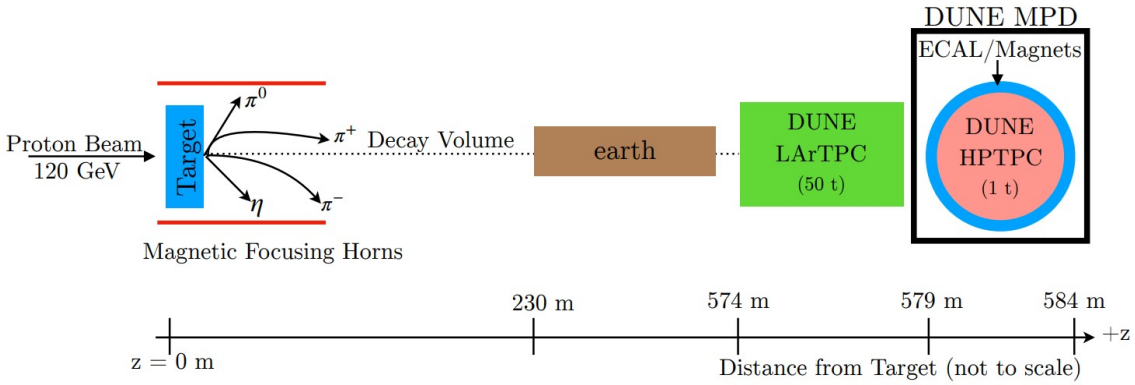

Figure 2.2: The DUNE multi-purpose near detector. The z-axis represents the beam direction; z = 0 m is the front of the target, z = 574 m corresponds to the front of the liquid argon detector, and z = 579 m is the front of the multi-purpose detector [32]

A block of concrete and steel is used to block the μ, but the ν_μ act like ghost particles and pass through the μ blocker. This focusing structure is optimized to provide a wideband neutrino beam with an energy range between 0.5 - 5 GeV, which includes the first two neutrino oscillation maxima. Therefore, we are left with high-intensity neutrino beams that pass through the near detector, that eventually pass through 1,300 km inside the crust of the earth and then into the enormous liquid-argon detector underground in South Dakota. By switching the horns to select and focus particles with the negative electric charge, we can also produce a beam of $\bar{\nu}_\mu$ [33]. Figure 2.2 shows the schematic of the DUNE near detector.

CHAPTER 3

MiniBooNE ANALYSIS

3.1 Study of Background and Simulation

By Beam Dump mode or Off-Target mode, we mean, the protons are not shot at the Beryllium target directly, but rather at an angle slightly away from the target, so that the beam just scrapes off the target in order to minimize the production of neutrinos. But, due to the high energy of the protons, they produce other particles that could be the postulated particles of BSM. As mentioned above, those processes will occur on the beamline and produce Z' bosons. To search for such Z' bosons, we use GEANT simulation packages to simulate the events inside the target and the detector. These simulations are generated via Monte Carlo Simulation Techniques and thus, enough events could represent the actual physics happening inside the detector.

For MiniBooNE, we have the data generated by simulation package BooNEG4Beam as given in Reference [34]. To study this data we first clearly define the signals and the backgrounds.

3.1.1 Backgrounds

There are two categories of backgrounds: i) beam-related and ii) beam-unrelated.

- Beam-related backgrounds:

  Since we are looking for photon events or electron/positron-like events, the neutrinos are the background to our study. All neutrino species and other particles whose final states are photons or electron/positron are the beam-related backgrounds. Beam-related backgrounds are contributed by detector events and events due to interaction with dirt.

- Beam-unrelated backgrounds:

  The beam-unrelated backgrounds are measured by a 2 Hz (10-15 Hz) random trigger for

off-target running and scaled by the ratio of number of beams triggers with POT delivered to the number of random triggers. The beam-unrelated background is more significant for off-target mode. Thus, the data-taking rate was increased for off-target mode.

3.1.2 Signals

The Z' gauge bosons couple with neutrino species and then decay into electron/positrons and photons in the detector. Thus, the signal we are looking for will have photon or electron/positron-like final states.

3.1.3 Data analysis and event selection

All PMT hits occurring within the trigger window comprise a beam event. The events in the MiniBooNE detector are recognized by the Cerenkov radiation and light scintillation produced in the mineral oil. Cerenkov radiation is electromagnetic radiation emitted when a charged particle (electrons, muons, etc.) passes through a dielectric medium at a speed greater than the phase velocity of light in that given medium. The Cerenkov radiation is more prominent and used mainly for detection. Electron candidates produce fuzzy and short rings inside the detector, while muons candidates produce a sharp outer ring with a fuzzy inner region. Pions produce two fuzzy rings inside the detector. We use this information to reconstruct the events for data collection and analysis. Both the electrons and muons assume a single particle track defined by seven parameters: $X = (t_0, x_0, y_0, z_0, \theta_0, \phi_0, E_0)$. The first four parameters are the four-vertex (time and three spacial origin points), the next two are the direction with the polar axis defined with respect to the beam axis ($\theta_0, \phi_0 \equiv U_x, U_y, U_z$), and the last is the energy [35].

3.1.4 Particle identification: Electron/Muon separation

First, we apply the preliminary cuts to eliminate cosmic backgrounds (by requiring the minimum number of PMT hits in the main region to be > 200 and the number of veto hits to be < 6). Then, apply the log-likelihood technique for particle identification in the detector. Furthermore, the average time of hits is required to lie within the expected beam delivery window from the Booster. We fit the quantities to obtain the maximum likelihoods that can be used for hypothesis

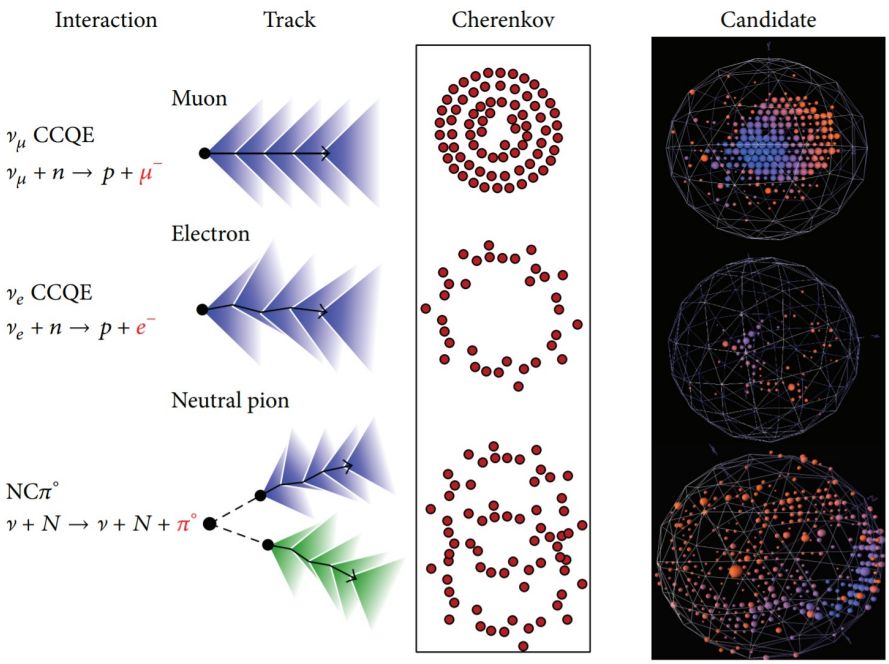

Figure 3.1: Particle identification in the MiniBooNE detector by using Cerenkov radiation

testing. We define two qualities:

$$\mathcal{R}_{e/\mu} \equiv \log \frac{\mathcal{L}_e}{\mathcal{L}_\mu} = \log \mathcal{L}_e - \log \mathcal{L}_\mu \tag{3.1.1}$$

$$\mathcal{R}_{e/\pi} \equiv \log \frac{\mathcal{L}_e}{\mathcal{L}_\pi} = \log \mathcal{L}_e - \log \mathcal{L}_\pi \tag{3.1.2}$$

are used to determine for a given event whether the electron hypothesis is preferred over the muon and π^0 hypothesis. In these expressions, $\mathcal{L}_e$, $\mathcal{L}_\mu$, and $\mathcal{L}_\pi$ are the maximized likelihoods returned by the electron, muon, and (fixed-mass) two-track fits, respectively [36].

There are two ideas to keep in mind when discussing the efficacy of selection cuts: sample efficiency and purity. The former is the fraction of all signal events that remain in the sample after selection cuts. The latter is the fraction of the sample made up by signal events. The criterion we use for filtering out the electron-like events from the reconstructed events is that in a single event, the likelihood of the electron hypothesis must exceed that of the muon hypothesis, i.e. $\log(\mathcal{L}_e/\mathcal{L}_\mu) \geq 0$.

CHAPTER 4

RESULTS AND FURTHER PROGRESS

4.1 Z' Production Result

The study of production and decay of Z' bosons for the DUNE near detector on both $L_\mu - L_e$ and $L_\mu - L_\tau$ has already been done in Reference [32].

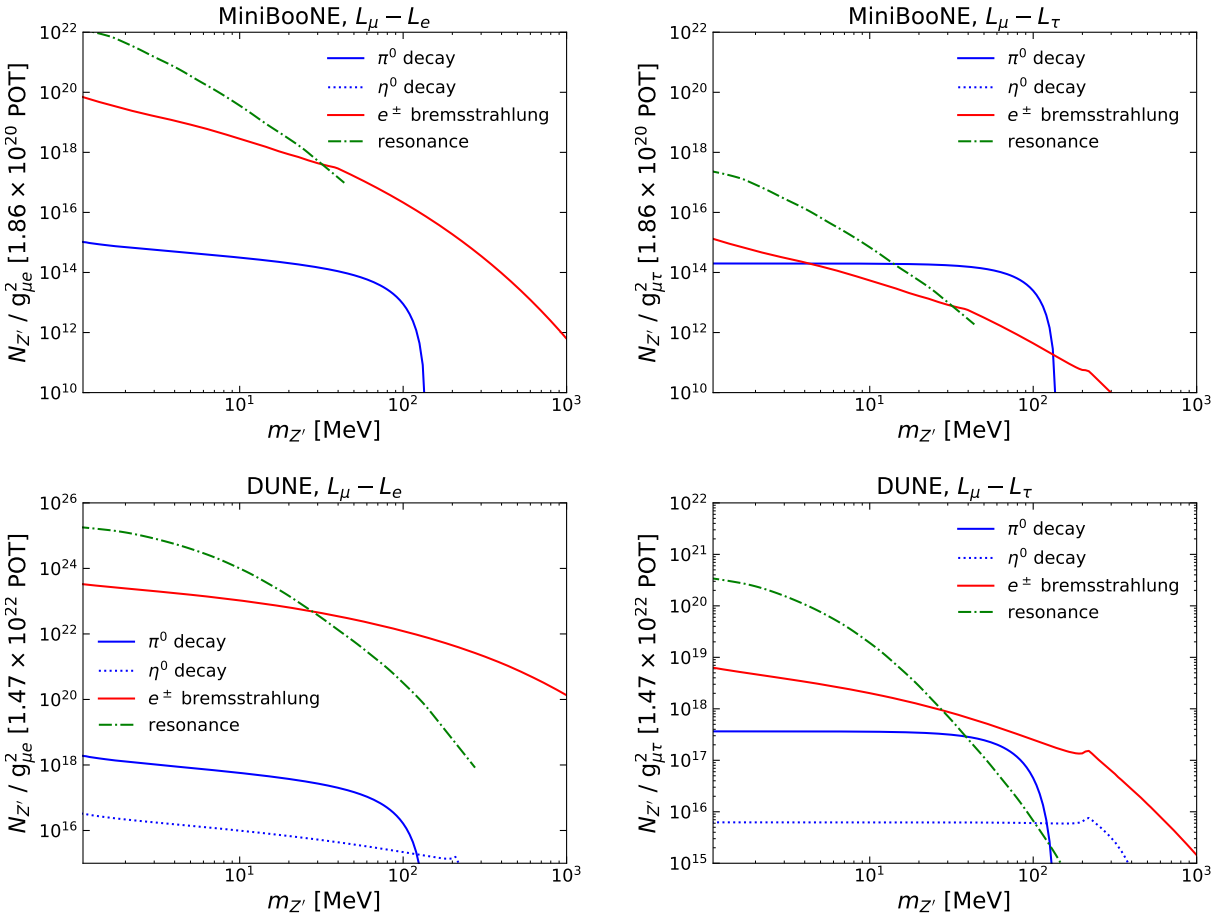

Figure 4.1: (Top) Number of Z' entering the MiniBooNE detector, as a function of $m_{Z'}$ for each production channel. The left panel refers to $L_\mu - L_e$, whereas the right one refers to $L_\mu - L_\tau$. (Bottom) Same as the panels in the top row, but for DUNE

We add to the study by making improvements on the expected number of Z' along with similar work for the MiniBooNE beam dump. The main distinction and improvement in our study from the mentioned literature lie in the production channels of Z'. We considered the main channels as the electron-positron bremsstrahlung and on-shell resonant production while in Reference [32] most of Z' comes from charged meson decays.

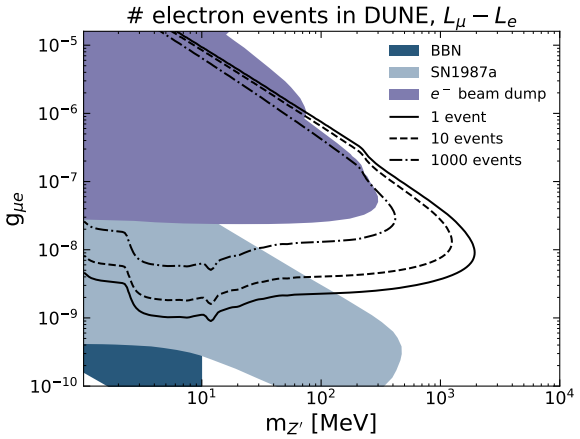

(a) $g_{\mu e}$ vs $m_{Z'}$ with the number of electron events.

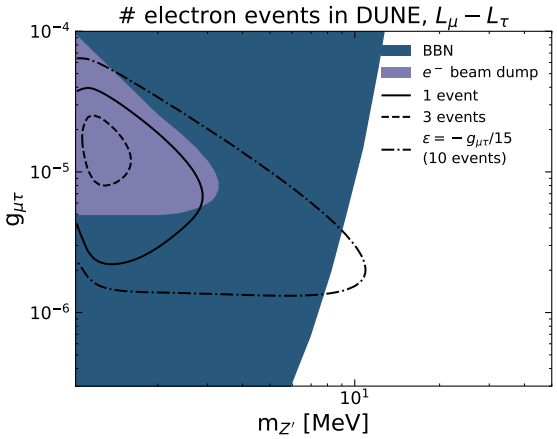

(b) $g_{\mu\tau}$ vs $m_{Z'}$ with the number of electron events.

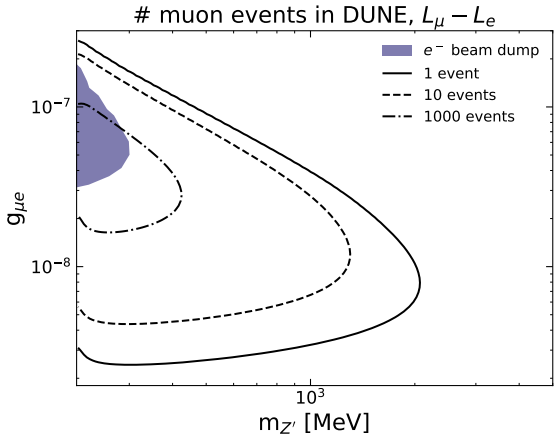

(c) $g_{\mu e}$ vs $m_{Z'}$ with the number of muon events.

Figure 4.2: The number of electron(muon) events in the DUNE near detector by the decay of Z' as a function of $m_{Z'}$. $g_{\alpha\beta}$ are the coupling constants with respect to gauged $L_\alpha - L_\beta$. The solid filled areas represent the region of the parameter space already excluded by the electron beam dump experiments SN1987a [37] and BBN [38]

.

We note that for $L_e - L_\mu$ we find that the number of Z' produced in the target is five orders of magnitude larger than the one connected to charged mesons estimated in Reference [32]. We

can see this by contrasting the number of $N_{Z'}$ produced for $L_e - L_\mu$ for DUNE in Reference [32] and Figure 4.1. Such a substantial increase in the number of Z' boson is because the process $\pi^\pm \to e^\pm \nu_e Z'$ and $\pi^\pm \to \mu^\pm \nu_\mu Z'$ (and a similar process for kaon) will contribute to the production of Z'. The decays involving electrons are helicity suppressed relative to those involving muons, which are also at suppressed rates. Thus, neutral meson decay is significant.

The number of Z' from charge mesons is similar to the one from electrons as seen on comparison for $L_\mu - L_\tau$ in Figure 4.1 and the same in Reference [32]. This happens because the charged meson decays involving muons are not suppressed by kinetic mixing, whereas suppression is indeed present for both the bremsstrahlung and resonant channels. This significant increase in the number of Z' suggests that DUNE can improve current constraints in the parameter space ($m_{Z'}$, $g_{\mu e}$) shown in Figure 4.2.

4.2 Current Progress and Future work

The search of Dark Matter in Beam Dump was initially done in Reference [34]. However, that search was for leptophobic DM models with a mass ranging between 5-50 MeV/c^2. Our search is for leptophilic DM Z' gauge bosons. We aim to analyze the beam dump data for the signature of photon-like or electron/positron-like final states.

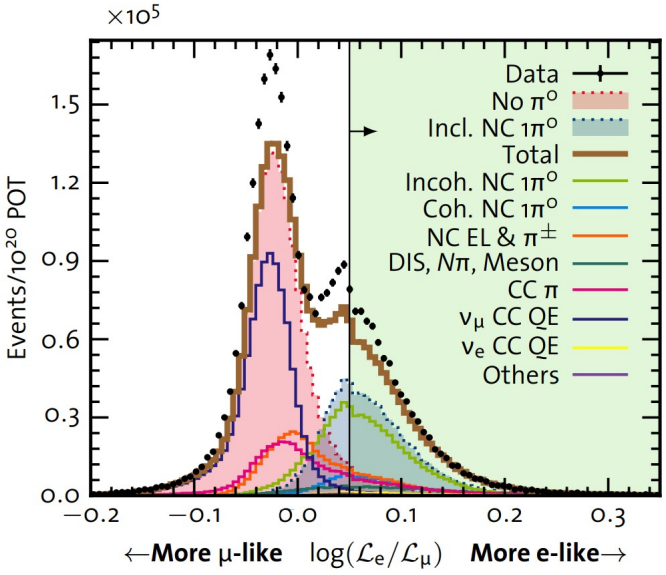

Figure 4.3: $\mathcal{R} = \log(\mathcal{L}_e/\mathcal{L}_\mu)$ distribution. The distribution includes events passing the preliminary cut in neutrino mode and anti-neutrino mode. $\log(\mathcal{L}_e/\mathcal{L}_\mu) > 0.01$ are electron-like events whereas to the left of it are the muon-like events

We have started to analyze the Monte Carlo (MC) Data for studying the efficiencies of different cuts. The analysis applies a similar technique using log-likelihood. The distribution of different neutrino species after the preliminary cut has been shown in Figure 4.3 [35].

In Figure 4.4 and Figure 4.5, we plot the efficiency of the electron-like and π^0-like particles in the final state selection cut in a 2-D histogram (binned scatter-plot) respectively. This allows us to analyze the efficiency of the cut in terms of energy and scattering angle in each individual bin. Thus, we can determine any anomalies in the data from the expected Monte Carlo easily. In the

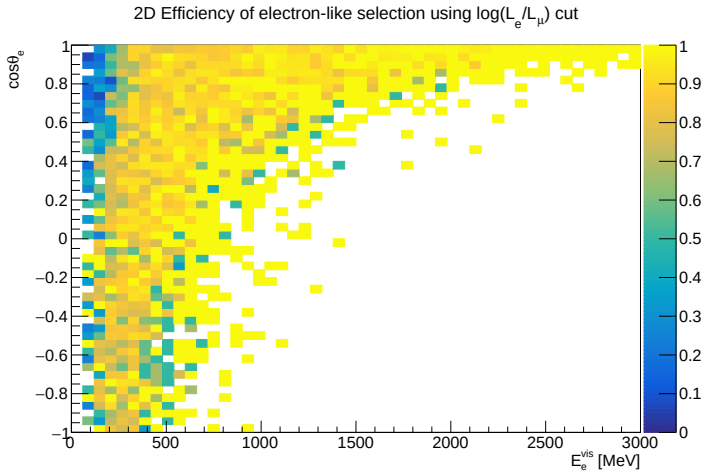

Figure 4.4: 2D histogram showing the efficiency of the electron-like event selection $\log(\mathcal{L}_e/\mathcal{L}_\mu) > 0.01$ cut

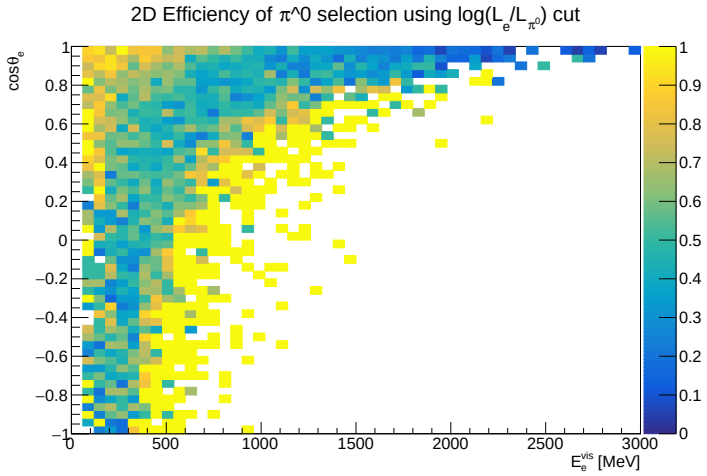

Figure 4.5: 2D histogram showing the efficiency of the π^0-like event selection $\log(\mathcal{L}_e/\mathcal{L}^0_\pi) < 0.01$ cut

top panel of Figure 4.6, we have plotted the efficiency of the cut as a function of electron visible energy or electron scattering angle. We see from the plot that the efficiency of the selection cut is above 90% for the electron visible energy above 350 MeV and the selection cut for electrons has an efficiency roughly averaging to 85% for any given electron scattering angle. The fit line for the efficiency curve as a function of electron visible energy is of the form given by Efficiency $=$ $A\ \arctan(B \cdot E_e^{vis}) + C$. Where, $A = p0$, $B = p1$, and $C = p2$ are given in the top left plot in Figure 4.6. The fit function for the efficiency curve as a function of electron scattering angle is of the form given by Efficiency $= A + B \cdot \cos\theta$. Where $A = p0$ and $B = p1$ are given in the top-right plot in Figure 4.6.

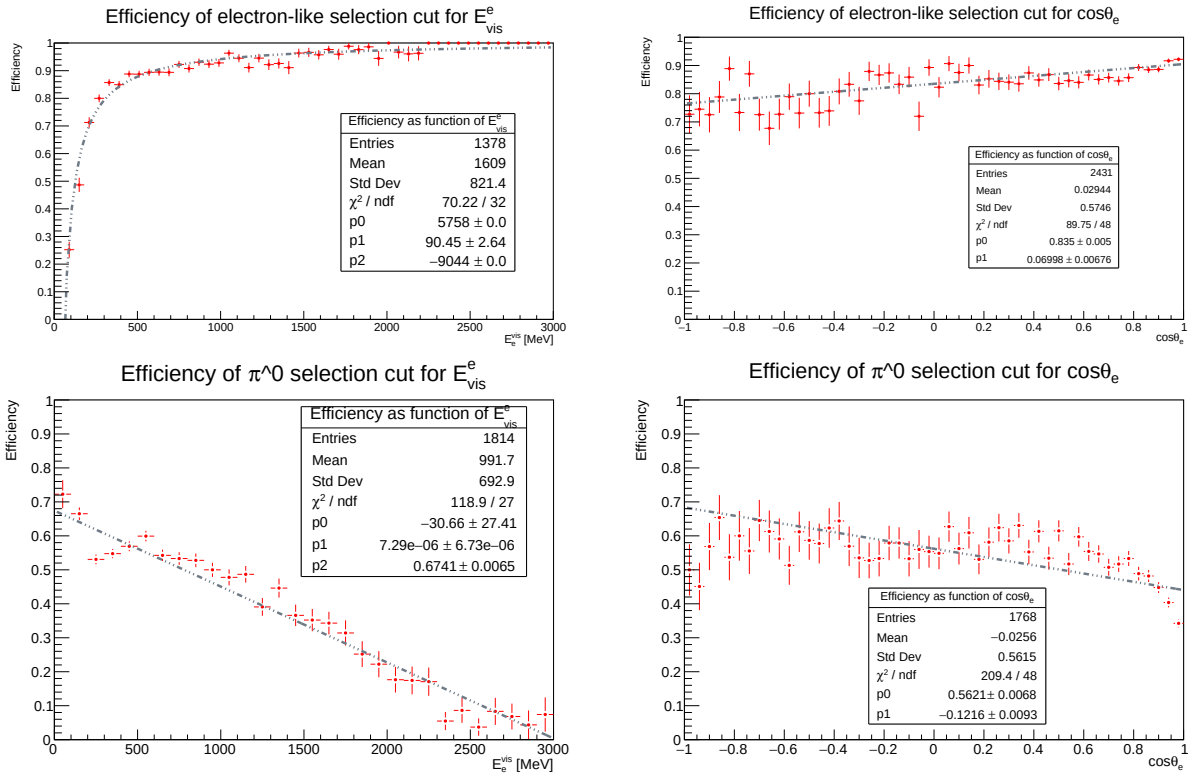

Figure 4.6: (Top) The efficiency of the particle selection cut for electron-like final states as a function of i) electron visible energy (left) and ii) cosine of the scattering angle of the electron (right). (Bottom) Same as the panels in the top row, but for particle selection cut for π^0-like final states

In the bottom panel of Figure 4.6, we have plotted the efficiency of the π^0-like event selection cut as a function of electron visible energy or electron scattering. The fit line for the efficiency curve as a function of electron visible energy is of the form given by Efficiency $=$

$A\ \arctan(B \cdot E_e^{vis}) + C$. Where, $A = p0$, $B = p1$, and $C = p2$ are given in the bottom left plot in Figure 4.6. The fit function for the efficiency curve as a function of electron scattering angle is of the form given by Efficiency $= A + B \cdot \cos\theta$. Where, $A = p0$ and $B = p1$ are given in the bottom right plot in Figure 4.6.

CHAPTER 5

CONCLUSION

In this paper, we have attempted to show that there is a significant number of Z' gauge bosons produced in the neutrino experiments like MiniBooNE and DUNE. We have shown that the number of Z' in the DUNE near detectors is quantitatively improved to what was previously expected by accounting for resonance production and electron and positron bremsstralung. This is substantial because it reconfirms that DUNE could also probe the Dark Sector of the SM and may detect new particles and give rise to new physics. Also, this suggests the DUNE near detector would be able to rule out all of the allowed region of $(g-2)$ in a $L_\mu - L_\tau$ model, with additional signatures from Z' decays to look for. Furthermore, the analysis of the data of the MiniBooNE beam dump will provide better cross section information for the search of Z' gauge bosons in the DUNE near detector.

APPENDIX A

FORCES IN THE STANDARD MODEL

The three forces of Nature together provide the foundation of the Standard Model (SM). In mathematical language, these forces are characterized by a group

$$G = SU(3) \times SU(2) \times U(1) \tag{A.0.1}$$

where the 3×3 matrix fields of $SU(3)$ describe the strong force, and the 2×2 matrix fields of $SU(2)$ describe the weak force. However, rather surprisingly the fields of $U(1)$ do not describe the force of electromagnetism. Instead, they describe an "electromagnetism-like" force that is called the *hypercharge*. The combination of $SU(2)$ and $U(1)$ is sometimes referred to as the *electroweak theory*.

APPENDIX B

ELECTRON-LIKE EVENT SELECTION PROCEDURE

For selecting the electron-like events (i.e. signal) from the data, we apply a cut in the data. The cut works on the hypothesis that the electron-like events and muon-like events in the data show different signatures in the detector. The fit applied at the Cerenkov radiation to an event in the detector gives a maximum likelihood value for the event to be electron (or muon), $\mathcal{L}_e$ (or $\mathcal{L}_\mu$). We take the logarithm of the ratio of $\mathcal{L}_e$ to $\mathcal{L}_\mu$. Then, when we plot the events, taking the $log(\mathcal{L}_e/\mathcal{L}_\mu) \geq 0.01$ filters out all but the electron-like events. There is a level of efficiency associated with each cut. Here, we have found the efficiency of the cut $log(\mathcal{L}_e/\mathcal{L}_\mu) \geq 0.01$ as follows:

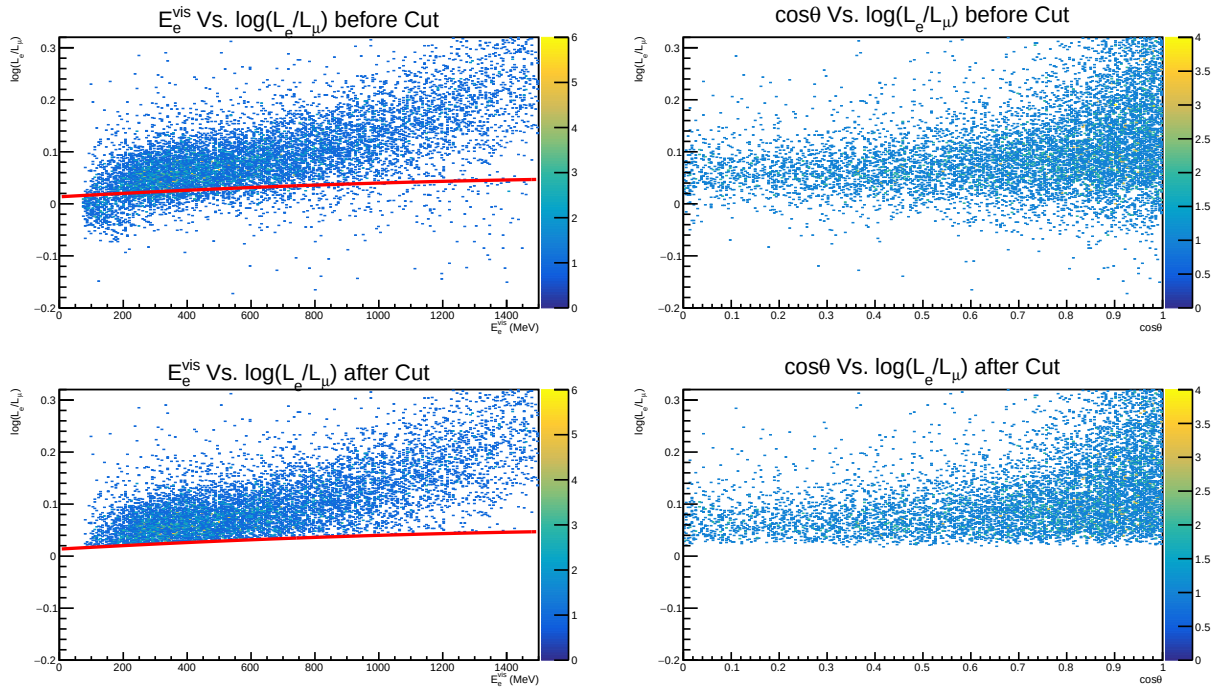

Figure B.1: Particle selection and efficiency of electron-like particle selection cut. The red line in the plot denotes the cut line. Above the red line are the electron-like events and below are the muon-like events. As we want electron-like events in the final states, we filter out the muon-like events and take the ratio between the histogram height in each bin to find the efficiency of the cut at each bin.

- First, we select the pure electron sample from the Monte Carlo data after the preliminary cuts, shown in the top two plots in Figure B.1.

- Then, we apply the cut to filter out only the electron-like events. The distribution of visible

energy or scattering angle of electrons after applying the cut is shown in the bottom two plots in Figure B.1.

- Finally, we take the ratio of the number of events in each bin after the selection cut and before the cut. This value is the efficiency of the cut for the given distribution of visible energy or scattering angle of electrons shown in the two bottom plots in Figure 4.3.

REFERENCES

[1] G. F. Giudice, P. Paradisi, and M. Passera, J. High Energ. Phys. **2012**, arXiv: 1208.6583, 113 (2012).

[2] Wu, Dan-di, (1991).

[3] A. A. Aguilar-Arevalo, B. C. Brown, L. Bugel, G. Cheng, J. M. Conrad, R. L. Cooper, R. Dharmapalan, A. Diaz, Z. Djurcic, D. A. Finley, and et al., Physical Review Letters **121** (2018).

[4] Y. Kaneta and T. Shimomura, Progress of Theoretical and Experimental Physics **2017** (2017).

[5] S. Gninenko and N. Krasnikov, Physics Letters B **783**, 24 (2018).

[6] M. Escudero, D. Hooper, G. Krnjaic, and M. Pierre, J. High Energ. Phys. **2019**, arXiv: 1901.02010, 71 (2019).

[7] X.-G. He, G. C. Joshi, H. Lew, and R. R. Volkas, Phys. Rev. D **44**, 2118 (1991).

[8] F. Capozzi, B. Dutta, G. Gurung, W. Jang, I. M. Shoemaker, A. Thompson, and J. Yu, arXiv:2108.03262 (2021).

[9] X.-G. He, G. C. Joshi, H. Lew, and R. R. Volkas, Phys. Rev. D **43**, R22 (1991).

[10] P. Ballett, T. Boschi, and S. Pascoli, JHEP **03**, 111 (2020).

[11] P. Coloma, E. Fernández-Martıénez, M. González-López, J. Hernández-Garcıéa, and Z. Pavlovic, Eur. Phys. J. C **81**, 78 (2021).

[12] M. Breitbach, L. Buonocore, C. Frugiuele, J. Kopp, and L. Mittnacht, (2021).

[13] M. Atkinson, P. Coloma, I. Martinez-Soler, N. Rocco, and I. M. Shoemaker, (2021).

[14] T. Schwetz, A. Zhou, and J.-Y. Zhu, (2021).

[15] K. J. Kelly, S. Kumar, and Z. Liu, Phys. Rev. D **103**, 095002 (2021).

[16] V. Brdar, B. Dutta, W. Jang, D. Kim, I. M. Shoemaker, Z. Tabrizi, A. Thompson, and J. Yu, Phys. Rev. Lett. **126**, 201801 (2021).

[17] B. Batell, M. Pospelov, and A. Ritz, Phys. Rev. D **80**, 095024 (2009).

[18] P. deNiverville, D. McKeen, and A. Ritz, Phys. Rev. D **86**, 035022 (2012).

[19] P. Coloma, B. A. Dobrescu, C. Frugiuele, and R. Harnik, JHEP **04**, 047 (2016).

[20] P. deNiverville and C. Frugiuele, Phys. Rev. D **99**, 051701 (2019).

[21] J. R. Jordan, Y. Kahn, G. Krnjaic, M. Moschella, and J. Spitz, Phys. Rev. Lett. **122**, 081801 (2019).

[22] A. de Gouvêa, P. J. Fox, R. Harnik, K. J. Kelly, and Y. Zhang, JHEP **01**, 001 (2019).

[23] V. De Romeri, K. J. Kelly, and P. A. N. Machado, Phys. Rev. D **100**, 095010 (2019).

[24] G. Magill, R. Plestid, M. Pospelov, and Y.-D. Tsai, Phys. Rev. Lett. **122**, 071801 (2019).

[25] P. Ballett, M. Hostert, S. Pascoli, Y. F. Perez-Gonzalez, Z. Tabrizi, and R. Zukanovich Funchal, Phys. Rev. D **100**, 055012 (2019).

[26] P. S. B. Dev, D. Kim, K. Sinha, and Y. Zhang, (2021).

[27] A. Celentano, L. Darmé, L. Marsicano, and E. Nardi, Phys. Rev. D **102**, 075026 (2020).

[28] P. Zyla et al. (Particle Data Group), PTEP **2020**, 083C01 (2020).

[29] B. Dutta, D. Kim, S. Liao, J.-C. Park, S. Shin, L. E. Strigari, and A. Thompson, (2020).

[30] E. Nardi, C. D. R. Carvajal, A. Ghoshal, D. Meloni, and M. Raggi, Phys. Rev. D **97**, 095004 (2018).

[31] A. A. Aguilar-Arevalo, C. E. Anderson, A. O. Bazarko, S. J. Brice, B. C. Brown, L. Bugel, J. Cao, L. Coney, J. M. Conrad, D. C. Cox, A. Curioni, Z. Djurcic, D. A. Finley, B. T. Fleming, R. Ford, F. G. Garcia, G. T. Garvey, C. Green, J. A. Green, T. L. Hart, E. Hawker, R. Imlay, R. A. Johnson, G. Karagiorgi, P. Kasper, T. Katori, T. Kobilarcik, I. Kourbanis, S. Koutsoliotas, E. M. Laird, S. K. Linden, J. M. Link, Y. Liu, Y. Liu, W. C. Louis, K. B. M. Mahn, W. Marsh, P. S. Martin, G. McGregor, W. Metcalf, P. D. Meyers, F. Mills, G. B. Mills, J. Monroe, C. D. Moore, R. H. Nelson, V. T. Nguyen, P. Nienaber, J. A. Nowak, S. Ouedraogo, R. B. Patterson, D. Perevalov, C. C. Polly, E. Prebys, J. L. Raaf, H. Ray, B. P. Roe, A. D. Russell, V. Sandberg, R. Schirato, D. Schmitz, M. H. Shaevitz, F. C. Shoemaker, D. Smith, M. Soderberg, M. Sorel, P. Spentzouris, I. Stancu, R. J. Stefanski, M. Sung, H. A. Tanaka, R. Tayloe, M. Tzanov, R. Van de Water, M. O. Wascko, D. H. White, M. J. Wilking, H. J. Yang, G. P. Zeller, and E. D. Zimmerman (MiniBooNE Collaboration), Phys. Rev. D **79**, 072002 (2009).

[32] J. M. Berryman, A. de Gouvea, P. J. Fox, B. J. Kayser, K. J. Kelly, and J. L. Raaf, JHEP **02**, 174 (2020).

[33] B. Abi et al. (DUNE), JINST **15**, T08008 (2020).

[34] A. A. Aguilar-Arevalo, M. Backfish, A. Bashyal, B. Batell, B. C. Brown, R. Carr, A. Chatterjee, R. L. Cooper, P. deNiverville, R. Dharmapalan, Z. Djurcic, R. Ford, F. G. Garcia, G. T. Garvey, J. Grange, J. A. Green, W. Huelsnitz, I. L. d. I. Astiz, G. Karagiorgi, T. Katori, W. Ketchum, T. Kobilarcik, Q. Liu, W. C. Louis, W. Marsh, C. D. Moore, G. B. Mills, J. Mirabal, P. Nienaber, Z. Pavlovic, D. Perevalov, H. Ray, B. P. Roe, M. H. Shaevitz, S. Shahsavarani, I. Stancu, R. Tayloe, C. Taylor, R. T. Thornton, R. Van de Water, W. Wester, D. H. White, and J. Yu, Phys. Rev. Lett. **118**, arXiv: 1702.02688, 221803 (2017).

[35] C. E. Anderson, *Measurement of muon neutrino and antineutrino induced single neutral pion production cross sections*, tech. rep. FERMILAB-THESIS–2010-49, 1000552 (May 2011), FERMILAB–THESIS–2010–49, 1000552.

[36] R. Patterson, E. Laird, Y. Liu, P. Meyers, I. Stancu, and H. Tanaka, Nuclear Instruments and Methods in Physics Research Section A: Accelerators, Spectrometers, Detectors and Associated Equipment **608**, 206 (2009).

[37] D. Croon, G. Elor, R. K. Leane, and S. D. McDermott, J. High Energ. Phys. **2021**, arXiv: 2006.13942, 107 (2021).

[38] M. Escudero, D. Hooper, G. Krnjaic, and M. Pierre, JHEP **03**, 071 (2019).

BIOGRAPHICAL INFORMATION

Gajendra Gurung is a senior undergraduate student from Nepal at the University of Texas at Arlington. He is majoring in Physics with a minor in Mathematics. Gurung will graduate with a Bachelor's in Science in December 2021. He plans on returning to the University of Texas at Arlington for a Ph.D. in Physics. He likes reading mystery novels, science fiction, and solving puzzles. Gurung's primary interest is in Particle Physics and Quantum Field Theory. In the spring of 2022, Gurung plans to go to CERN to work on the Deep Underground Neutrino Experiment under the supervision of Dr. Jaehoon Yu as a graduate student.